SUPPLEMENTARY MATERIAL FOR: Atomic-Scale Deformations at the Interface of a Mixed-Dimensional van der Waals Heterostructure

Kimmo Mustonen,[*,†] Aqeel Hussain,[‡] Christoph Hofer,[†] Mohammad R.A. Monazam,[†] Rasim Mirzayev,[†] Kenan Elibol,[†] Patrik Laiho,[‡] Clemens Mangler,[†] Hua Jiang,[‡] Toma Susi,[†] Esko I. Kauppinen,[‡] Jani Kotakoski,[†] and Jannik C. Meyer[*,†]

†*University of Vienna, Faculty of Physics, 1090 Vienna, Austria*

‡*Aalto University School of Science, Department of Applied Physics, P.O. Box 15100, FI-00076 Aalto, Finland*

E-mail: kimmo.mustonen@univie.ac.at; jannik.meyer@univie.ac.at

1. Non-cleaned heterostructures

Surface contamination originating from the CVD process, transfer and environment are a major concern for two-dimensional materials.[1,2] Despite our intrinsically clean synthesis process[3,4] and deposition[5] of single-walled carbon nanotubes (SWCNTs), the heterostructures fabricated on commercial CVD graphene were covered by contaminating material. Figure S1 shows how the samples typically appear prior to the high-power laser annealing.[6] In this particular case, the clean graphene spots, visible as dark contrast, are roughly 5–20 nm in size. While this is often enough for observation of 2D materials in their pristine state, it hinders the structural determination of SWCNTs and conceals the topographic features around them.

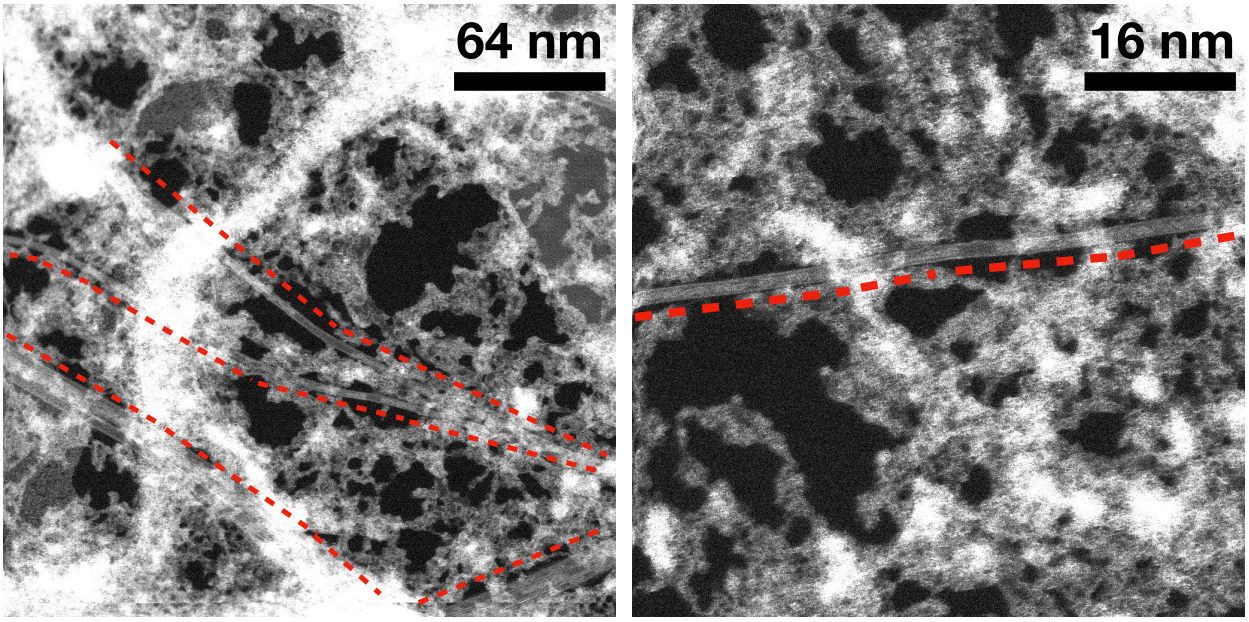

Figure 1: As-fabricated example of dry-deposited[5] single-walled carbon nanotubes[3,4] on commercial monolayer graphene from Graphenea Inc. The dark contrast in these images is clean graphene. To guide the readers' eye, the positions of carbon nanotubes are highlighted with red dashed lines.

2. Chiral index assignment for graphene-suspended carbon nanotubes

The assignment of chiral indices, (n, m), of a SWCNT by using *e.g.* transmission electron microscopy (TEM) in diffraction mode has many implementations.[7–13] A crude approximation is given by measurement of the diameter in real-space, and the chiral angle θ_{chiral} in reciprocal space through the use of electron diffraction.[13] All modern implementations, however, rely completely on the structural representation of a SWCNT in the reciprocal space, retrieving the structure based on the relative positions of the characteristic diffraction peaks.[10,12,14]

Here, instead of using electron diffraction, we calculate Fourier transforms (FTs) of real-space images thus converting them into reciprocal space. We first analyze the (n, m) of the SWCNT in manuscript Figure 1d and then test the robustness of our method to radial deformations. A real-space image of the tube is reproduced in Figure S2a and its FT in Figure S2b. The chiral indices are related to the structure of a tube in 3D reciprocal space, described by a set of Bessel functions.[9] These functions, when intersected by the Ewald's sphere, are represented by a number of layer lines that encode the structure of the tube. It has been independently shown that the layer line spacings are directly related to the chiral indices (n, m),[10] and so are the (squared) Bessel functions dominating the intensities along each layer line.[11,12] Figures S2c and S2d plot the intensity profiles along the layer lines L_1 and L_2. By measuring the relative distance of the first and second maxima we can determine the order of the Bessel function along the line by calculating $J_n(x) = X_2 \ / \ X_1$, yielding the chiral indices as tabulated in the original publication by Liu *et al.*[11] We can similarly use the layer line spacing, d_i, to calculate (n, m), for which the related intensity profiles are plotted in Figures S2e and S2f. The d_i is defined as a distance of each layer line from the equatorial line L_0, related to n and m through a set of geometric equations.[10] This method, however, is calibrated by the period of oscillation along the equatorial line, δ, proportional to the wall

separation of the tube only, rendering it susceptible to radial aberrations.

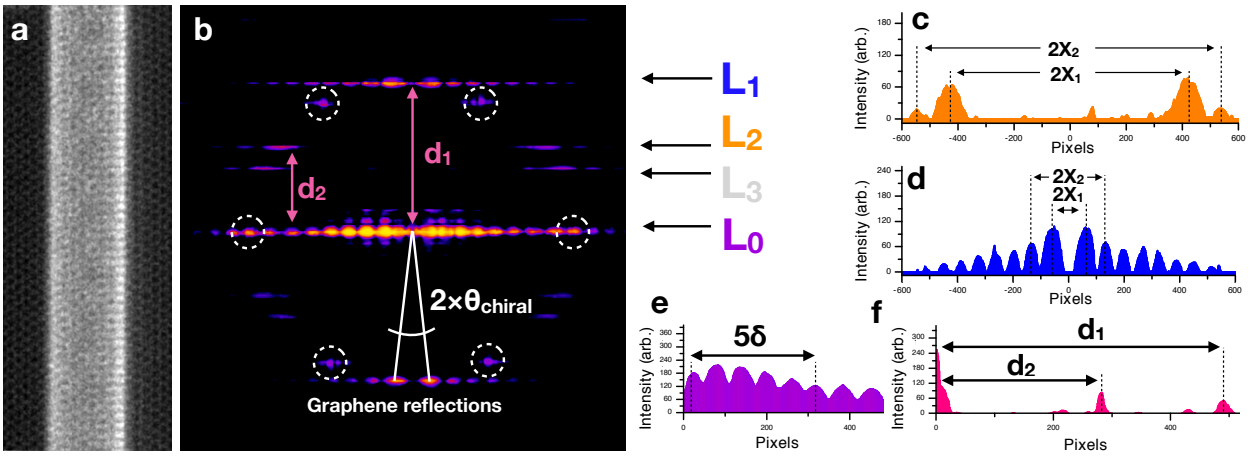

Figure 2: (a) Real-space image of the tube shown in manuscript Figure 1d and its Fourier transform in (b). The L_i and d_i mark the positions of layer lines and their distance from L_0. The intensity profiles along the layer lines L_1 and L_2 are shown in (c-d) and along the the equatorial line L_0 in (e). The intensity profile perpendicular to equatorial line is plotted in (f).

A calculation of X_2 / X_1 along L_2 yields 1.244 ± 0.005 and along L_1 2.202 ± 0.005 (uncertainties from peak positions). These values match best to $n = 20$ and $m = 2$, with a second best match of $n = 21$ and $m = 2$. Similarly, if we determine the structure using the d_i, we get $n = 20.39 \pm 0.1$ and $m = 1.95 \pm 0.1$.

To evaluate the robustness of the methods against radial deformations,[14] we determined the (n, m) for tubes simulated with an elliptical shape. Figures S3a-c show FTs of simulated $(20, 2)$ tubes radially compressed respectively by 0%, 3% and 6%. Starting with the circular case, we get X_2 / $X_1 = 1.246 \pm 0.001$ along L_2 and 2.177 ± 0.001 along L_1, matching almost perfectly to $n = 20$ and $m = 2$. Similarly, the layer line spacing yields $n = 20.00 \pm 0.01$ and $m = 2.01 \pm 0.01$.

For 3% and 6% compressed tubes we likewise acquire X_2 / $X_1 = 1.243 \pm 0.001$ and 1.243 ± 0.001 along L_2, and X_2 / $X_1 = 2.209 \pm 0.001$ and 2.182 ± 0.001 along L_1, respectively. The best structural match in both cases is $(20, 2)$ and the second best $(21, 2)$. From layer line spacing we get $n = 20.32 \pm 0.01$ and $m = 1.97 \pm 0.01$ for 3% compressed and $n = 20.52$ ± 0.01 and $m = 1.94 \pm 0.01$ for 6% compressed tube. It thus appears the layer line spacing is, as expected, somewhat sensitive to radial deformations. Nonetheless, at high confidence our example tube is indeed a $(20, 2)$ with only a small amount of eccentricity. For unclear cases of (n, m), however, it may become necessary to run extensive simulations to assign the correct structure. As an example of that, Figure S4 compares the experimental FT to the nearest matching indices showing that $(20, 2)$ is closer than $(21, 2)$. For comparison, we also show a FT of $(20, 3)$, having a similar diameter but distinct structure in the reciprocal space.

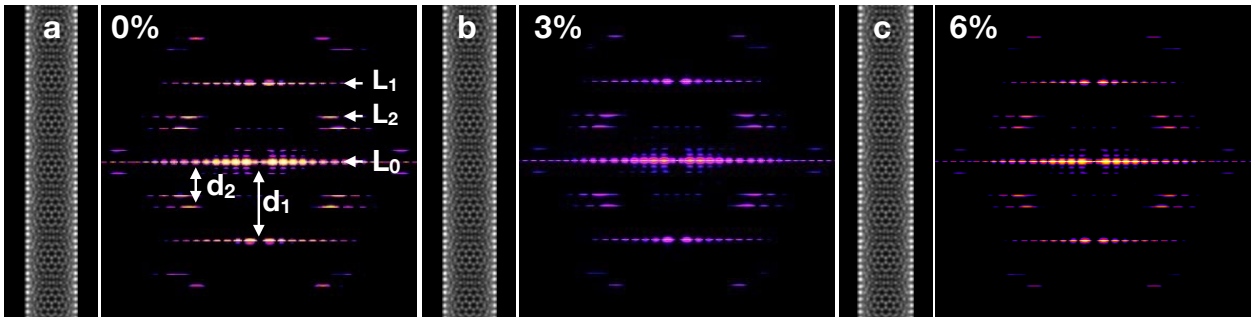

Figure 3: (a) A real-space image of a circular $(20, 2)$ tube and its Fourier transform. (b-c) 3% and 6% radially compressed $(20, 2)$ tubes with their corresponding Fourier transforms.

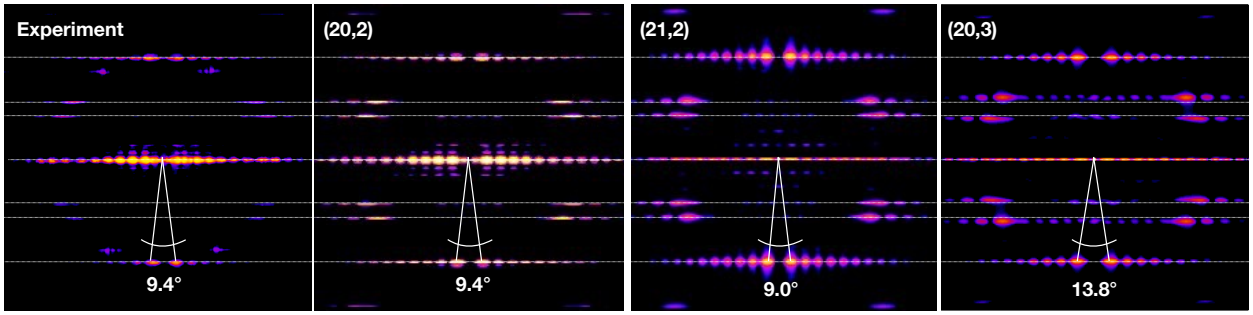

Figure 4: Comparison of the FT acquired from experiment to the closest matching chiral indices of $(20, 2)$ and $(21, 2)$. $(20, 3)$ is shown for comparison.

3. Adsorption energy and carbon nanotube eccentricity

The adsorption energy of a $(13, 3)$ SWCNT on graphene was calculated by compressing a pristine graphene supercell by 0.0-0.8% to introduce negative strain. The width of the graphene area in the cell was the same as in the main manuscript, ∼64 nm.

Here, we have normalized the adsorption energy and cell size by those of the non-compressed simulation cell. These normalized values are plotted in Figure S5, showing that when graphene is able to fold around the tube due to the negative strain, the nanotube shows larger deformation as measured by its eccentricity.

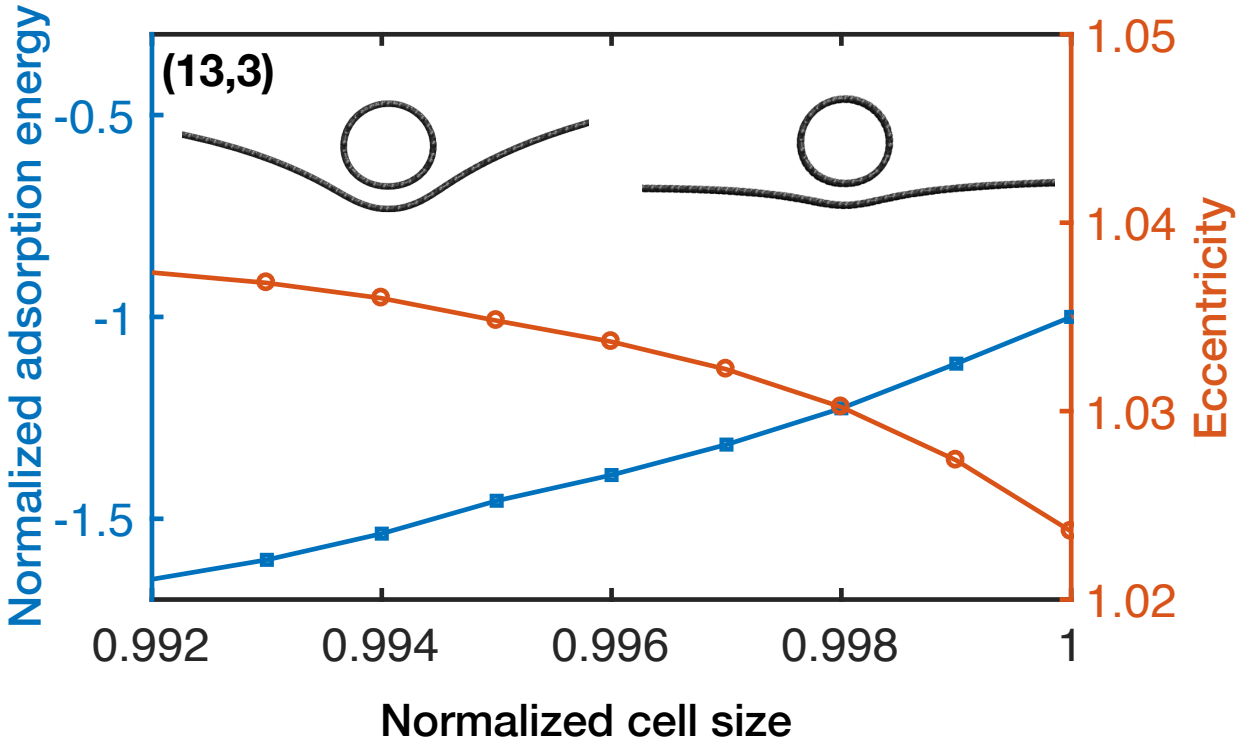

Figure 5: Normalized adsorption energy and eccentricity of a $(13, 3)$ SWCNT on graphene as a function of normalized simulation cell size. Atomistic models of the extremes are shown as insets.

References

1. Haigh, S.; Gholinia, A.; Jalil, R.; Romani, S.; Britnell, L.; Elias, D.; Novoselov, K.; Ponomarenko, L.; Geim, A.; Gorbachev, R. Cross-Sectional Imaging of Individual Layers and Buried Interfaces of Graphene-Based Heterostructures and Superlattices. *Nat. Mater.* **2012**, *11*, 764.

2. Rooney, A. P.; Kozikov, A.; Rudenko, A. N.; Prestat, E.; Hamer, M. J.; Withers, F.; Cao, Y.; Novoselov, K. S.; Katsnelson, M. I.; Gorbachev, R.; Haigh, S. J. Observing Imperfection in Atomic Interfaces for van der Waals Heterostructures. *Nano Lett.* **2017**, *17*, 5222–5228.

3. Mustonen, K.; Laiho, P.; Kaskela, A.; Zhu, Z.; Reynaud, O.; Houbenov, N.; Tian, Y.; Susi, T.; Jiang, H.; Nasibulin, A. G.; Kauppinen, E. I. Gas Phase Synthesis of Non-

Bundled, Small Diameter Single-Walled Carbon Nanotubes With Near-Armchair Chiralities. *Appl. Phys. Lett.* **2015**, *107*, 013106.

4. Hussain, A.; Liao, Y.; Zhang, Q.; Ding, E.-X.; Laiho, P.; Ahmad, S.; Wei, N.; Tian, Y.; Jiang, H.; Kauppinen, E. I. Floating Catalyst CVD Synthesis of Single Walled Carbon Nanotubes from Ethylene for High Performance Transparent Electrodes. *Nanoscale* **2018**, *10*, 9752–9759.

5. Laiho, P.; Mustonen, K.; Ohno, Y.; Maruyama, S.; Kauppinen, E. I. Dry and Direct Deposition of Aerosol Synthesized Single-Walled Carbon Nanotubes by Thermophoresis. *ACS Appl. Mater. Interfaces* **2017**, *9*, 20738–20747.

6. Tripathi, M.; Mittelberger, A.; Mustonen, K.; Mangler, C.; Kotakoski, J.; Meyer, J. C.; Susi, T. Cleaning Graphene: Comparing Heat Treatments in Air and in Vacuum. *Phys. Status Solidi RRL* **2017**, *11*, 1700124.

7. Bernaerts, D.; Zettl, A.; Chopra, N. G.; Thess, A.; Smalley, R. Electron Diffraction Study of Single-Wall Carbon Nanotubes. *Solid State Commun.* **1998**, *105*, 145–149.

8. Colomer, J.-F.; Henrard, L.; Launois, P.; Van Tendeloo, G.; Lucas, A.; Lambin, P. Interpretation of Electron Diffraction from Carbon Nanotube Bundles Presenting Precise Helicity. *Phys. Rev. B* **2004**, *70*, 075408.

9. Meyer, J. C.; Paillet, M.; Duesberg, G. S.; Roth, S. Electron Diffraction Analysis of Individual Single-Walled Carbon Nanotubes. *Ultramicroscopy* **2006**, *106*, 176–190.

10. Jiang, H.; Nasibulin, A. G.; Brown, D. P.; Kauppinen, E. I. Unambiguous Atomic Structural Determination of Single-Walled Carbon Nanotubes by Electron Diffraction. *Carbon* **2007**, *45*, 662–667.

11. Liu, Z.; Qin, L.-C. A Direct Method to Determine the Chiral Indices of Carbon Nanotubes. *Chem. Phys. Lett.* **2005**, *408*, 75–79.

12. Jiang, H.; Brown, D. P.; Nasibulin, A. G.; Kauppinen, E. I. Robust Bessel-Function-Based Method for Determination of the (n, m) Indices of Single-Walled Carbon Nanotubes by Electron Diffraction. *Phys. Rev. B* **2006**, *74*, 035427.

13. Lambin, P.; Lucas, A. Quantitative Theory of Diffraction by Carbon Nanotubes. *Phys. Rev. B* **1997**, *56*, 3571.

14. Liu, Z.; Qin, L.-C. Electron Diffraction from Elliptical Nanotubes. *Chem. Phys. Lett.* **2005**, *406*, 106–110.